ARCHIVIO ISTITUZIONALE
DELLA RICERCA

Alma Mater Studiorum Università di Bologna
Archivio istituzionale della ricerca

Tracing groundwater in a fractured arenitic aquifer by DNA-labelled, silica encapsulated nanoparticles in the Northern Apennines (Italy)

This is the final peer-reviewed author's accepted manuscript (postprint) of the following publication:

*Published Version:*
Pugliese, E., Giuliani, C., Bolognesi, G., Filippini, M., Barbero, M., Ehdaie, M., et al. (2025). Tracing groundwater in a fractured arenitic aquifer by DNA-labelled, silica encapsulated nanoparticles in the Northern Apennines (Italy). HYDROGEOLOGY JOURNAL, 33(6), 1607-1620 [10.1007/s10040-025-02939-7].

*Availability:*
This version is available at: https://hdl.handle.net/11585/1023790 since: 2026-02-05

*Published:*

DOI: http://doi.org/10.1007/s10040-025-02939-7

*Terms of use:*

Some rights reserved. The terms and conditions for the reuse of this version of the manuscript are specified in the publishing policy. For all terms of use and more information see the publisher's website.

This item was downloaded from IRIS Università di Bologna (https://cris.unibo.it/).
When citing, please refer to the published version.

(Article begins on next page)

05 September 2026

# Tracing groundwater in a fractured arenitic aquifer by DNA-labelled, silica encapsulated nanoparticles in the Northern Apennines (Italy)

Ernesto Pugliese[1], Cristina Giuliani[1], Giorgia Bolognesi[2], Maria Filippini[1], Matteo Barbero[1], Marjan Edhaie[1], Alessandro Gargini[1*]

1. *Biological, Geological and Environmental Sciences Department, Alma Mater Studiorum University of Bologna, 40126, Italy*
2. *Medical and Surgical Sciences Department, Alma Mater Studiorum University of Bologna, 40126, Italy*

**corresponding author, E-mail: alessandro.gargini@unibo.it*

**ORCID identifiers**:

Ernesto Pugliese: 0009-0003-1707-8875

Cristina Giuliani: 0000-0002-5318-6502

Giorgia Bolognesi: 0000-0002-7296-6897

Maria Filippini: 0000-0001-5050-5072

Alessandro Gargini: 0000-0002-9271-219X

**Keywords**: DNA-labelled nanoparticles • tracer tests • fractured/macroporous systems • Italy • Northern Apennines

**Abstract**

A field tracer test using DNA-labelled silica encapsulated nanoparticles was conducted in an arenitic fractured aquifer. The hydrogeological context involves a primary discharge outlet of the Pantano Formation, a shallow marine arenite serving as a crucial groundwater reservoir for the mountainous region of the metropolitan area of Bologna (Northern Apennines, Italy). The aquifer's characteristics, including calcarenite composition prone to karstification and the enlargement of sedimentary and tectonic discontinuities, were conducive to showcasing the ability of nanoparticles ability to trace preferential flow pathways within a dual-porosity aquifer. Nanoparticles were introduced into a borehole and retrieved from three sampling points: two spring-boxes and another borehole. The distances between injection and retrieval points ranged from 5-15 m in planar projection and 12-63 m in linear depth. Additionally, a NaCl tracer test with similar boundary conditions was conducted during a borehole dilution test. DNA concentration was determined through quantitative polymerase chain reaction (qPCR) following the dissolution of the silica shell using a buffered fluoride etch solution. Complete breakthrough curves for nanoparticles were observed in all three sampling points, with early detection and nearly symmetrical curves at the two closest points, suggesting minimal dispersion effects. In contrast, salt tracing resulted in more dispersed and delayed breakthroughs. The median

effective groundwater velocity from the tracer tests was one order of magnitude higher compared to literature data on siliciclastic turbiditic sandstones in the Northern Apennines. These findings hold significance for implementation of protection measures around the spring head.

## 1. Introduction

The DNA molecule presents numerous potential advantages in tracing groundwater flow systems compared to classical tracers such as ionic solutions or fluorescent dyes (Leibungdut et al. 2009). These advantages include: specificity (i.e. minimizing effects from background noise particularly for use of synthetic DNA), full compatibility with environment (Mora et al. 2015), ultra-sensitivity to analysis with much lower detection limits compared to ionic or dye tracers, and potential for multi-tracer tomography-like assessment (Sharma et al. 2012; Liao et al. 2018). DNA-based tracer tests, utilizing the molecule as an organic solute dissolved in groundwater, have demonstrated numerous advantages in tracking water flow pathways, either from the first applications in column experiment in the lab (Grindrod et al. 1996; Mikutis et al. 2018) or across various hydrological compartments, from septic pollution sources in sewers system (Georgakakos et al. 2019; Pang et al. 2017) to surface waters (Foppen et al. 2011, 2013) and glaciated systems (Dahlke et al. 2015). Nonetheless, the application of the technology for hydrogeological purposes in field conditions is still at the stage of a novelty, due to some significant drawbacks that hinder its widespread application: degradability of DNA molecule, with a half-life of less than 10 h at 20°C in aquatic environment, and possible absorption/retardation processes, a feature that is not entirely compatible with long transit times in the porous medium (Mikutis et al. 2018).

In the rapidly evolving field of applied hydrogeology, the advent of nanotechnology has ushered in a new era of possibilities. Nanoparticles offer unprecedented tools for a better comprehension and management of groundwater resources through their application in tracer tests, resulting in significantly enhanced specificity and sensitivity (Divine & McDonnell 2005; Sharma et al. 2012). Nanoparticles can be designed, produced and utilized not only to act as tracers by themselves, as seen in the case of zero-valent iron particles (Chuang et al. 2016), but also to enhance the capabilities of organic molecules such as synthetic DNA which can be encapsulated and protected within nanoparticles (McNew et al. 2018; Mikutis et al. 2018; Wang & He 2010). The encapsulation of DNA within a silica nanoparticle shell, facilitated by nanotechnology, has recently improved the application potential of tracer tests in porous and fractured media. The main advantage associated with this technology includes the resistance of the DNA molecule to physical and chemical stresses thanks to the protection offered by the outer silica shell. Moreover, there is no experimental evidence of negative interference with other classical tracers used concurrently. Finally, the slightly negative surface charge of the particles enhances their mobility thanks to an attenuation of surface effects along pore walls (Zhuang et al. 2009).

Silica-encapsulated nano particles must indeed be considered as colloidal tracers, typically in the size range 10-1000 nm (Matthess 1982); the hydrodynamic behavior of nanoparticles in a porous medium thus resembles contamination by viruses or bacteria more than contaminants in solute phase (Harvey & Garabedian 1991). Nanoparticles behave as an advection dominated tracer, transported more rapidly and spending less time in the porous medium compared to a solute tracer (Albarran et al 2013; Dahlke et al 2015; Kittilä et al 2019; McKay et al. 2000; Mikutis et al 2018). As macroclastics are transported in high velocity channels throughout rivers so

nanoparticles, acting as a selective tracer, provide specific information on larger flow conduits. Also the low recovery rate of nanoparticles is an indicator of preferential transport only along high-permeability flow paths.

However, drawbacks are also evident, including gravity settling (James & Chrysikopoulos 2011) and pore size exclusion effects due to the colloidal nature of the particles and the constraint that pore throats must be at least 1.5 times larger than the particle size to permit their passage (Sirivithayapakorn & Keller 2003). The preferential migration along the flow paths with higher groundwater velocity could lead to a poor representativeness of the bulk dispersion properties of the porous medium. Additionally, the high cost of this particles compared to classical tracers and the need for interdisciplinary facilities that merge field hydrogeology and molecular biology approaches must be considered. Table 1 provides a synthetic review of DNA-based tracer hydrogeological applications in field conditions either as solute DNA molecules or encapsulated in nanoparticles.

This research is based upon a collaboration among hydrogeologists and molecular biologists to provide the first application of a tracer test utilizing DNA-labelled silica-encapsulated nanoparticles in an arenitic fractured aquifer. The investigated aquifer is characterized by a peculiar karst-like enlargement of primary or secondary discontinuities and represents a strategic groundwater reservoir for public water supply. As demonstrated by the results of the investigation, properties of nanoparticles proven as well suited to put in evidence some specific features of the investigated aquifer.

## 2. Hydrogeological setting and reasons for tracing

The tracer test was performed in a fractured sedimentary aquifer located in the central sector of the Northern Apennines (Northern Italy) around 40 km to the south west of the city of Bologna (Fig. 1a). The Apennines are a Neogenic fold-thrust belt formed from the collision between the African and Eurasian tectonic plates during the Alpine orogenesis (Carminati & Doglioni 2012). The Northern branch of the chain extends along a front approximately 350 km long, defining the divide between watersheds draining toward the Adriatic sea to the north and those ones draining toward the Ligurian sea to the south (Fig. 1a). The chain is formed by piles of rock units (nappes) overthrusted between each other. From a lithological standpoint, the orogenic structure is underlain by a metamorphic Paleozoic bedrock and is made up by a Mesozoic calcareous succession, followed by pelagic shales and turbidites and, at the structural top, by the Ligurid units, primarily composed by mudstones, clayey complexes and scattered arenitic slabs deposited in “piggyback basins” over the Ligurid units themselves (Castellarin 2001). Unlike the Central and Southern Apennines, extending farther south along the italian peninsula and where the Mesozoic limestones outcrop at the structural culmination of the chain due to the erosion of the overlying sedimentary units, in the Northern sector which is characterized by relatively lower altitudes the shallowest and outcropping geological portion consists of turbidites, arenites and clayey complexes.

**Table 1** Main parameters of DNA tracer tests performed on the field in different hydrogeological settings. The depth is reported in m below ground level (bgl). The meaning of $v_{e\text{-}max}$ (first arrival) and $v_{e\text{-}p}$ (peak arrival) is explained in the main text. The Gradient indicates with *N* (No) an active pumping of groundwater at the sampling site; with *Y* (Yes) not perturbed conditions. The DNA indicates with *Y* (Yes) encapsulation of molecule, whereas *N* (No) indicates free DNA molecule as solute.

| Reference | Aquifer porosity | Litology | Injection depth (m bgl) | Traced distance range (m) | Test duration range (h) | $v_{e\text{-}max}$ velocity (m/d) | $v_{e\text{-}p}$ velocity (m/d) | Gradient | DNA | Mass Recovery (%) |
|---|---|---|---|---|---|---|---|---|---|---|
| Colleuille & Kitterød (1998) | Interstitial | Coarse sand and gravel | 13 | 50-300 | 3-12 | 260-2400 | 104 | N | Y | - |
| Kitterød et al (1998) | Fractured | Gneiss | - | 180 | 5-20 | 864 | - | Y | Y | - |
| Sabir et al (1999) | Interstitial | Sand | 2 | 12 | 5 | 3,1 | - | N | Y | - |
| Sabir et al (1999) | Fractured | Amphibolite | 15.5 | - | 0.23-68 | 12-2074 | - | N | Y | - |
| Ptak et al (2004) | Interstitial | Sand and gravel | - | 13 | 0.33 | 946 | 125 | N | N | - |
| Dahlke et al (2015) | Fractured/ Karst | Glacier mass | - | 226-313 | 0.18-0.3 | 25,040 – 29,585 | 6,780-7,907 | Y | Y | 46-77 |
| Aquilanti et al (2016) | Karst | Limestone | 0 | 1,800-2,000 | 62-417 | 114-702 | - | Y | N | 6-57 |
| Kong et al (2018) | Interstitial | Sandy gravel with finer matrix | - | 3 | 0.42 | 171.4 | 57.6-58.4 | Y | Y | - |
| Kittilä et al (2019) | Fractured | Granodiorite | - | 6.5-28.7 | 3.8-4.4 | 42-156 | 24.4-60.8 | N | Y | 2.7-59 |
| Pang et al (2020) | Interstitial | Coarse gravel | - | 21-87 | 2-22 | 74-252 | 55-168 | Y | Y-N | - |
| Pang et al (2020) | Interstitial | Fine sand | - | 0.5-3 | 36 | 0.01 | 0.01 | Y | N | - |

Due to this geological differentiation, hydrogeological research in the Northern branch of the Apennines is primarily focused on sedimentary aquifers, while karst limestone massifs are the primary objects of investigation in the rest of the chain (Petitta et al. 2022). The most common groundwater reservoirs in Northern Apennines are turbidites, either siliciclastic or calcareous, or ophiolites (peridotites and basalts embedded inside the Ligurid units), which are mainly used to provide water supply for local communities or small villages. Significant spring discharges (i.e. between 1 and 0.01 L/s in low flow condition, corresponding to a Meinzer's flow rate magnitude classes VI-VII; Meinzer 1923) are rare and are typically related to very localized geological and geomorphological settings (Gargini et al. 2008; Segadelli et al. 2021).

Within this context of relatively limited groundwater resources, some springs discharge at higher rates (up to Class IV Meinzer's flow rate magnitude, between 10 and 100 L/s), attracting the interest of water companies and hydrogeological researchers (Filippini et al. 2024). These springs discharge from the Pantano Formation ("PAT" in official geological maps), an arenite pertaining to the Epiligurian succession. The Epiligurian succession is a series of Cenozoic marine formations deposited, from the Middle Eocene to the Upper Miocene, in settings ranging from shallow shelf to slope, within "piggyback basins" (Ori & Friend 1984) formed above the predominantly argillaceous Ligurid units. The PAT unit forms high standing slabs ranging from 2 to 25 $km^2$, surrounded and hydrogeologically limited by permeability barriers, thus forming separate aquifer reservoirs. One of these slabs, called "Arpolli", is the focus of this investigation, showing a total outcropping area of approximately 3 $km^2$

(Fig.1b). The PAT unit, being a shallow marine formation, exibits variability in lithological and textural features depending on the depositional environment, ranging from proximal one (nearshore with more calcarenitic composition) to distal at the edge with slope facies (Bettelli et al. 2002; Panini et al. 2002). Slabs formed by the more proximal facies, such the Arpolli slab, consist primarily of calcarenites made up of very fine to medium-size grey sands with gross parallel-plain layering locally including microconglomerates. The content of calcite is high both in the clasts and in the cement of the rock denoting a massive appearance in outcrop (Fig.1c).

The main spring discharge outlets of the slab are located at its western edge, at a permeability threshold along a sub-vertical fault putting in contact the PAT unit to the east with a marly aquitard of Epiligurian succession (Cigarello Formation; *"CIG*" to the west (Fig.1 b, d). Along this boundary, two main discharge points are located, known as the Arpolli spring group (Site A in Fig.1 b, d and hereafter) and the Canevaccia spring (Site C in Fig. 1 b). The two have a total mean annual discharge and a mean low flow season discharge of 28 and 14 L/s, respectively, based on a monthly monitoring performed during the hydrological year 2020/2021. The major discharge point is A site where a total of 6 spring-boxes (coded from *S1* to *S6* in Fig.3a) are exploited for public water supply, providing a yearly averaged discharge of 24 L/s, which is significant for the general hydrogeologic context of the Northern Apennines.

The presence of the aforementioned spring-boxes and two boreholes drilled within the spring discharge area of Site A (see *The tracer test: Setting, materials and methods*) has provided the opportunity to conduct either a borehole/spring or a borehole/borehole tracer test (Käss 1998) within a primary discharge area of a fractured sedimentary aquifer aiming to experimentally verify the degree of hydrologeological connectivity within such a peculiar aquifer.

## 3. The tracer test: Setting, materials and methods

The six spring boxes of Site A are situated within an area of approximately 3 ha (Fig.2a). They consist of shallow vertical shafts reaching the water table at around 2 m below ground level (bgl), or of horizontal draining tunnels 10-15 m long at a depth of 2 m bgl (Fig.3). The primary purpose of all spring-boxes is to facilitate groundwater drainage by gravity, from the aquifer toward a nearby reservoir building (*R* in Fig.2) via buried pipes. For detailed characterization of the fractured aquifer at Site A and for groundwater monitoring purposes, the company responsible for aqueduct supply (Gruppo Hera S.p.A.) drilled two boreholes, B1 and B2, in close proximity to the spring-boxes at a distance of 10 m between them and down to a depth of 80 and 33 m bgl, respectively (Fig.2, Fig.3). Prior to completion with open-stand pipe piezometers, the two boreholes underwent acoustic and optical televiewer vertical logging. As part of a parallel research effort aimed at hydrodynamically characterizing the PAT unit in the broader Bologna region, constant flow rate pumping tests lasting 8 hours were conducted inside the boreholes. Technical and hydrogeological details of the spring boxes and boreholes are provided in Table 2.

| ID | Altitude (m asl) | Inner Ø (inches) | Depth (m bgl) | Screen (m bgl) | Depth to GW (m bgl) | *Q* (L/s) | *T* ($m^2/s$) | *K* (m/s) |
|---|---|---|---|---|---|---|---|---|
| B1 | 796 | 3 | 80 | 49-80 | 2.18-1.16 | - | $4\times10^{-3}$ | $1\times10^{-4}$ |
| B2 | 795 | 3 | 31 | 2-31 | 2.02-0.89 | - | | |
| S2 | 794 | - | 3.35 | - | 1.20 | 6.7-6.6 | - | - |
| S3 | 793 | - | 2.80 | - | ~2 | 6.5-7.3 | - | - |

**Table 2** Technical features of groundwater points and relevant associated hydrogeological parameters. Explanation of terms and symbols: *ID*: identification code of groundwater point; *Altitude* is referred to ground surface; *Depth to GW* is referred to depth to water-table with the range of values occurring during the two tracer tests; *Q*: spring discharge with the range of values occurring during the two tracer tests; *T*: hydraulic transmissivity; *K*: hydraulic conductivity. Parameters *T*, *K* were obtained by pumping tests on B1 and B2.

The lithology log obtained from continuous coring revealed the presence of the arenitic unit of PAT down to 80 m depth. The lithology is made up by a layered, lithologically homogeneous calcarenite with grain sizes ranging from medium to coarse sands and up to fine gravels. Downhole observations using acoustic and optical televiewer logging allowed the identification of fractures with aperture of 5-15 cm, located at depths 27.50-28.50 m depth and again in discrete clusters between 61 and 80 m depth bgl. Fractures are developed along a WNW-ESW direction (Fig.3) with a dip of 200° and a slope of 65-70°. Additionally, other enlarged fractures were observed

along the separation surfaces of the layers (layer-parallel fractures). Enlarged fractures/conduits show a reddish-brown alteration coating of precipitated material, indicating active groundwater flow enhancing rock dissolution (Barker et al, 1998).

Within this setting two distinct tracer tests were conducted with a 4-month interval between them. DNA-labelled nanoparticles were utilized as tracer while the other employed NaCl. For both tests the borehole B1 served as the injection point whereas three recovery points were designated for the retrieval of the tracer breakthrough curve (BTC). These are two spring boxes (S2 and S3) and one borehole (B2). The location of all points, along with the indication of the linear distances between them, is shown in Fig.2b. Local groundwater flow is directed northward with a local hydraulic gradient of $7.8\times10^{-2}$.

### *3.1 DNA-labelled silica nanoparticles*

Double-stranded synthetic DNA-labelled silica nano particles were injected in borehole B1. Nanoparticles were manufactured and quality controlled, according to Paunescu et al (2013), by the Swiss Federal Institute of Technology (Zürich, CH). The used DNA is a random sequence with a length of 65 base pairs (bp):

"TACTCGCTGCTGTGACTGACGACTCGACTCATAGTGAATAGTGACCGGTAGACCTGCTGAACCTA"

encapsulated into amorphous silica spheres (nanoparticles) that protect the organic molecule from physical and chemical stresses. Before encapsulation the inner nucleus of silica nanoparticles was functionalized, by the producer, with N-trimethoxylsilylpropyl-N,N,N-trimethylammonium chloride (TMAPS) in order to obtain a positively charged surface on silica and non-covalently bind DNA molecule to it. In the end the DNA was coated with an outer thin layer of silica (encapsulating shell) by polycondensation of tetraethoxysilane (TEOS) (Stöber process). The DNA loading of a single particle is ≈ 0.1% in weight. The primary particle diameter is ≈ 150 nm (range 140-170 nm) with a density of around 2 mg/mm$^3$ (2 kg/dm$^3$), corresponding to twice the density of fresh water; consequently, a single particle has a mass of around $3.5\times10^{-12}$ mg. Concerning the size, nanoparticles constitute a colloidal tracer. The original manufactured material is dispersed in water (1 mg/mL) and a total amount of 1 mg of material includes around 280 billion ($2.8\times10^{11}$) individual primary particles. The manufacturing procedure of Paunescu et al (2013) was found to produce agglomerated clusters of particles so about 1-2 orders of magnitude lower is the expected number of particle aggregates travelling across the porous medium after injection (Robert Grass, Swiss Federal Institute of Technology, Zürich, personal communication).

### *3.2 Tracer injection*

***3.2.1 DNA***: a mass of 0.5 milligrams of nanoparticles, dispersed in 9.5 mL of deionized water (DNA concentration of 1 µg/mL), was introduced into borehole B1 in correspondence of the middle point of the screened sector at 65 m bgl. This quantity corresponds to an approximate number of $1.4\times10^{11}$ nanoparticles, with a concentration of 1 µg/mL DNA. The total injected mass of DNA was 9.5 µg. Forcing an instantaneous pulse injection of such a small quantity of tracer at depth in groundwater was a critical issue therefore an air pressure flash pump was specifically designed for the test (Fig.3): at ground surface the pulse at 8 atm was provided by a compressed air tank (AT in Fig.3) connected down the hole, through a flexible Rilsan® tubing (4 mm inner ⌀), with a steel injection chamber assisted with a pressure valve. The injection chamber was charged with the tracer and lowered into the borehole down to the desired depth. For the very low size of injected volume (9.5 mL) and the adopted modality the injection could be reasonably approximated to a pulse injection (Dirac Delta function).

***3.2.2 NaCl***: the tracer injection was performed through a borehole dilution test (BDT) following the permeable bag method (Fahrmeier et al, 2021; Piccinini et al, 2016). A non-woven fabric permeable bag filled with 1 kg of fine-grained NaCl was lowered and lifted for three times along the screened interval of B1. The complete dissolution of NaCl occurred rapidly within the borehole. Vertical logging of specific electrical conductance (SEC) was performed immediately before and during the test using a profiler probe (model: Solinst TLC 107, with compensation at 25°C). The background SEC prior to injection was 468 µS/cm (average of ten regularly spaced measures of the vertical log along the screened sector in the range 463-473 µS/cm).

### *3.3 Tracer sampling*

***3.3.1 DNA***: sampling was performed in different ways according the typology of water point: for springs S2 and S3, samples were collected every 10 min from injection directly at the final outlet of the pipe conveying, by gravity, the uptaken groundwater to the aqueduct's local reservoir (R in Fig.2); for borehole B2, each 15 min, by lowering a bailer down inside the water column along the screened sector. Two bailers were used alternatively. Before insertion each bailer was accurately rinsed many times with spring water (pristine aquifer water) discharged from one of the outlets located upgradient respect to the injection point. 10 mL groundwater aliquots were collected in 15 mL Falcon tubes after accurately rinsing the cap and container twice.

***3.3.2 NaCl:*** in the BDT the breakthrough of the ionic tracer was determined by measuring SEC in springs S2 and S3, and in borehole B2. In S2 and S3 a field conducimeter (Hanna HI991301 with compensation at 25°C) was used to monitor SEC at the outlet pipe conveying water from the springs in the R facility. SEC was measured every 35 min in general (lower frequency respect to the sampling of nanoparticles). In B2, SEC was monitored through five vertical logs, performed in general every 35 min with the first one after 55 min from injection, using the same profiler adopted in B1 (also in B2 the blank SEC profile was determined immediately before the injection). The SEC values recorded immediately before injection (background) were 516 and 519 µS/cm at S2 and S3, respectively; a blank value of 475 µS/cm for point B2 resulted as the average of thirteen regularly spaced measures of the vertical SEC log along the screened sector of the borehole (range between 456 and 496 µS/cm). In summary, SEC background values at the site ranged between 456 and 519 µS/cm, taking also into account the values detected in B1.

### *3.4 Laboratory analysis of DNA*

Each 10 mL groundwater sample containing the DNA-labelled silica particles was concentrated by transferring 1000 µL of sample into a 1.5 mL tube, centrifuging at maximum speed for 3 min at room temperature and discarding the supernatant; the procedure was repeated 10 times to exhaust the sample. Successively, the dissolution of silica shells, and the consequent release of the DNA in aqueous solution, was obtained by adding 45 µL of a fluoride-containing solution (buffered oxide etch, BOE), at pH 4, obtained by dissolving 0.23 g of ammonium hydrogen difluoride ($NH_4FHF$) and 0.19 g of ammonium fluoride ($NH_4F$) in 10 mL of $H_2O$ inside a polyethylene container. Lastly, a dilution 1:100 of the samples in water was performed in order to minimize the tendency of the residual of etching solution to limit quantitative polymerase chain reaction (qPCR) detection (Panescu et al, 2013; Mikutis et al, 2018). The dissolved DNA was directly used for qPCR reaction without any purification.

The analysis of DNA was performed by qPCR (StepOnePlus Real-Time PCR, Applied Biosystems), an instrument that simultaneously amplifies and quantifies a specific DNA sequence, using the fluorescent dye SYBR Green as follows: 10 µL of Power SYBR Green PCR Master Mix (Applied Biosystems); 1 µl of forward primer (10 µM); 1µl of reverse primer (10 µM); 3µL of Real-Time PCR water; 5 µL of DNA template. The following Real-Time PCR cycling parameters were used: 95°C for 10 min (pre-activation), 95°C for 15 s, 54°C for 30 s, and 72° C for 30 s (40 cycles; Paunescu et al, 2013). The primers used were TACTCGCTGCTGTGACTGAC (forward primer) and TAGGTTCAGCAGGTCTACCG (reverse primer). As part of each experiment, three no template controls (NTC) consisting of water instead of DNA were included. Samples were analyzed using three real-time PCR replicates.

The measurement obtained by qPCR for each replicate is the theshold cycle (Ct), indicating the number of amplification cycles required for the fluorescent signal emitted by the SYBR Green to be detected by the instrument (Kong et al, 2018). To ensure accuracy of the analyses, the following rules for managing Ct values were applied: if the standard deviation (SD) of the Ct values of the triplicates was less than 0.5, the mean of the three Ct values was calculated and the sample was kept for a further analysis; if the SD was greater than 0.5, the sample was subjected to a new analysis in triplicate; if a couple of replicates showed a SD of less than 0.5, the mean of the two Ct values was considered as the real value of the sample. Subsequently, the triplicate of NTC was used to establish the minimum detection threshold and filter out samples, as "no DNA detected" or "negative samples", with a Ct mean higher than the detection threshold.

In order to correlate the mean Ct value to the DNA concentration in the samples, for each experiment (sampling site) a regression line (dilution curve) was preliminarly constructed in the laboratory using serial dilutions of DNA at known concentration (0.33 ng/µL concentrated stock solution) and the mean Ct values associated to each dilution (Panescu et al, 2013). Specifically, seven 1:10 serial dilutions from the stock solution were prepared with a concentration range between $3.3\times10^{-2}$ ng/µL and $3.3\times10^{-8}$ ng/µL.

The equation of the obtained regression line and the mean Ct value of each sample were then used to derive the DNA concentration. The minimum detectable concentration (limit of detection of DNA) was defined equal to $2.64\times10^{-11}$ g/L (equivalent to $2.64\times10^{-2}$ ng/L or ppt), corresponding to an estimated total number of 37 particles; this limit is calculated according to the lowest Ct mean value obtained from the "negative samples". So to any concentration lower than this limit down to "null" was assigned a label of "non detected".

## 4. Results and discussion

In this chapter the obtained breakthrough curves (BTC) are described and interpreted along with the derivation of the main physical parameters like the components of groundwater effective velocities or the kinematic porosity, so emphasizing the observation approach to derive the hydrodynamic properties of the arenites and to make comparisons between DNA and NaCl; no modelling of the curves will be provided. The BTCs are reported in Fig.4, in comparative way, with the concentration of DNA expressed in ng/L and the SEC in µS/cm as the differential respect to the blank of each sampling site. The curves connecting the points relative to the detected concentrations in the BTCs in Fig.4 must be considered simply a graphic support to the observation and interpretation of the graphs and do not represent the actual pattern of the tracer recovery between the points.

However the high time frequency of the sampling (10 min for DNA) makes this graphic representation more realistic. The exact location of a peak or of a first detection are not precisely known and all the following estimates encompasses this intrinsic uncertainty also if we consider not altered the general conclusions about the observations of the experiment.

### *4.1 Breakthrough curves from nanoparticles*

BTCs were observed at each of the three sampling points (Fig. 4). The first tracer detection occurred very early at the first sampling step at all three points (10-15 min after injection) and likewise fast was the attaining back to values below the detection limit (between 180 and 240 min after injection). A clear peak was recorded in S2 and B2, followed by a more or less decreasing tail of the BTC, with the maximum concentration (5.44 ng/L) detected in S2, the nearest point to the injection site. In S2 the main peak was followed, 80 min later, by a secondary peak around the same level of concentration of the main peak detected in B2 (respectively 1.84 and 1.31 ng/L). The peaks detected in S2 and B2 are related to transport of nanoparticles along main fractures with different velocities. The shape of the BTC registered in S3 looks notably less structured, showing scattered values above and below the detection limit with a relatively low maximum concentration of 0.19 ng/L recorded 60 min after injection; S3 spring-box has a very long draining-tunnel inlet respect to the point type of S2 and B2 and this likely damps the signal.

The total injected mass of DNA was 9.5 μg. Integrating the BTCs allowed estimation of a recovery of 9.9%. Mass recovery was strongly unbalanced with the dominant proportion in S2 (9.40% of the total mass) and a very low fractions at the other two points (0.5 and 0.02% in S3 and B2, respectively).

### *4.2 Borehole Dilution Test (BDT) and breakthrough curves from NaCl*

The BDT in B1, acting as the injection pulse of the NaCl tracer, was monitored through nine vertical SEC profiles performed every 30-35 min. In Fig. 5 the profiles are represented, for each measuring depth, as a differential value respect to the pristine SEC. The relevant SEC drop over time (indicative of NaCl dilution) are observed along the depth intervals 53-56 and 75-80 m bgl. Both intervals correspond to or are nearby high-aperture fractures observed inside the borehole through optical and acoustic televiewer logging (as put in evidence in Fig.5). As observed by the upward inflection of SEC curves at the top of the screened sector of the borehole, the injection of NaCl did not determine the complete release of the complete mass of the tracer. Instead, a fraction of NaCl mass, during the descent phase of the permeable bag, likely was dissolved in the upper non-screened sector of the borehole so representing a continuous source by molecular diffusion toward the sector below involved in the active groundwater flow. The effect of this delayed release of NaCl was not relevant for the interpretation of BDT (after the injection the complete recovery of the original ionic concentration inside the water column was achieved in 5 hours, as observed in Fig.5) but had effects on the obtained breakthrough curves at the recovery points as previously mentioned.

Breakthrough curves of differential SEC values relative to background levels were observed at each of the three sampling points (Fig. 4). For NaCl, the tracer detection began at the first sampling step after injection in all three points (30 min for S2, S3 and 90 min for B2). Due to the effects of delayed NaCl release from the upper not-screened sector of B1, described in *Tracer injection*, and to the lower temporal resolution of NaCl sampling, the pattern of BTCs are rougher than those of the nanoparticles. For S2 and S3 springs BTCs fail to represent the

whole distribution of the recovered tracer down to background SEC values and their pattern resembles more to the tracer arrival from a continuous injection stabilizing up at a sort of a plateaux. In contrast, at the B2 borehole, the BTC returns to background SEC values.

### *4.3 Groundwater effective flow velocities*

The groundwater effective flow velocity ($v_e$), e.g. the actual velocity of water particles inside a porous medium, commonly expressed by a single bulk value (the average linear velocity, obtained by the ratio of the Darcian, or apparent, velocity **q** and the effective porosity $n_e$; Fetter, 2018), should actually be expressed by a statistical distribution of values reflecting the pores/fractures size distribution. The BTC of a tracer transported by groundwater is a reliable proxy of this distribution because it is affected by the contribution of different flow velocities from the injection to the recovery point. Following the conceptual model of a generic breakthrough curve proposed by Käss (1998), the following relevant values of groundwater effective velocities can be derived. These are calculated as the ratio between the linear distance $L$ from the injection point to the recovery point, and the tracer arrival time $t$ at the recovery point, as detected in the BTC: (1) the maximal effective velocity ($v_{e\text{-}max}$), corresponds to the first arrival time of a tracer (the first value higher than the detection limit); (2) the dominant (peak) effective velocity ($v_{e\text{-}p}$), corresponds to the arrival time of the maximum detected tracer value; and (3) the median effective velocity ($v_{e\text{-}med}$), corresponding to the arrival time at which half of the recovered tracer mass has been observed. For the estimation of $v_{e\text{-}med}$, the complete recovery of the tracer down back to the background value is required.

The obtained ranges of values of the groundwater effective velocities from the BTCs at the site, expressed in m/d, are presented (Fig.6); each component of the velocity is expressed as a range between the maximum and minimum values obtained, for each type of tracer, from the three recovery points. The value of $v_{e\text{-}max}$ is between 2190 and 662 m/d, for nanoparticles, and between 730 and 162 m/d, for NaCl; the value of $v_{e\text{-}p}$ is between 970 and 221 m/d, for nanoparticles, and between 438 and 74 m/d, for NaCl (for nanoparticles the values range of $v_{e\text{-}p}$ relative to the second delayed peak clearly observed in all recovery points is between 199 and 60 m/d); the value of $v_{e\text{-}med}$ is between 380 and 170 m/d, for nanoparticles, and 105 m/d for NaCl (calculated only for B2 BTC where the SEC returns to the pristine value).

In comparison with other traced sandstone aquifers in Northern Apennines, groundwater effective velocity values obtained by using fluorescent dyes by Vincenzi et al, (2009, 2014) in siliciclastic or calcareous turbidites are shown in Fig.6. These tests were performed exploiting the hydraulic connection between streams and excavated tunnels for train transportation. Tracer tests were performed where arenites are more dominate than pelites in the turbidite sequence. The velocities detected from PAT at the A site were systematically higher with respect to those obtained in turbidites, up to more than one order of magnitude.

### *4.4 Kinematic porosity*

Through the combination of the results obtained by a BDT and tracer test, a range of values for the kinematic porosity of the arenitic unit could be provided. The apparent or Darcian groundwater flow velocity (**q**) was derived from the BDT, according the method reported in Fahrmeier et al. (2021), obtaining a value of $8.9\times10^{-6}$ m/s (0.77 m/d) equal to the product of the hydraulic conductivity multiplied by the hydraulic gradient. This represents the water velocity value inside the borehole, relative to the zones with the higher salt dilution (Fig.5) and directed along the local hydraulic gradient. The kinematic porosity ($n_k$) value could be estimated as the ratio between $q$ and $v_{e\text{-}med}$ obtained from the BTCs of adopted tracers. The $n_k$ value associated to nanoparticles is in the range 2.0-4.5‰ (corresponding to the $v_{e\text{-}med}$ range of 380-170 m/d) whereas the one from NaCl is equal to 7.3‰ (corresponding to a $v_{e\text{-}med}$ value of 105 m/d).

### *4.5 Comparison of parameters among tracers*

Nanoparticles were observed to move more rapidly compared to solute tracers, confirming that their migration is limited to larger flow paths associated with faster flow velocities, as previously documented by various authors (Bailly-Comte et al 2018; Chrysikopoulos & Katzourakis 2015; Mikutis et al. 2018; Zvikelsky et al. 2008; Sabir et al., 2001). The ionic tracer exhibits retarded transport: for instance the second peak of concentration detected in S2 for nanoparticles (likely related to a fracture system with lower aperture) is also replicated by the NaCl BTC, but more delayed and dispersed (Fig.4). The lower values of $n_k$ derived from nanoparticles reflect the aforementioned preference for preferential flow paths for this type of tracer, with only a small fraction of the total kinematic porosity available for effective flow. Comparable values of $n_k$ for sandstones, obtained by tracer tests, are reported by Medici et al (2016).

## 5. Conclusions

Groundwater flow in a fractured aquifer was succesfully traced by DNA-labelled silica-encapsulated nanoparticles at a scale of a few tens of meters under non-perturbed conditions. This report represents the first documented application of this tracer test performed with such a tracer in an arenitic fractured aquifer. An injection of 0.5 mg of nanoparticles (containing 9.5 μg of synthetic DNA) was performed via air pressure at 65 m bgl inside a borehole, and resulted in breakthrough curves at three different sampling points represented by two springs and one borehole. The first tracer detection was rapid (≤10 min after injection), and background concentrations were backer-established within 3 to 4 hours. The shape of the BTCs in the two nearest sampling points seem to indicate a very low dispersivity of the tracer and transport of particles dominated by secondary discontinuities. A tracer test with NaCl was performed in the same injection and recovery points. A comparison between the dynamics observed for the two tracers confirms the aptitude of nanoparticles to trace preferential flowpaths due to their colloidal nature.

Nanoparticles behave as an advection-dominated tracer, transported more rapidly and spending less time in the porous medium compared to the solute tracer. Just as macroclastics are transported in high velocity river channels, nanoparticles, acting as a selective tracer, provide specific information on larger flow conduits. In addition, the low recovery rate of nanoparticles is an indicator of preferential transport along high-permeability flow paths, due to the size exclusion effect of colloidal particles from smaller fracture throats or to the effect of gravity sedimentation through pathways of irregular shape and high tortuosity. Analogous results using colloidal tracers have been reported in the literature (Albarran et al 2013; Dahlke et al 2015; Kittilä et al 2019; Mikutis et al 2018).

The aptitude of nanoparticles to limit their effectiveness in tracing only higher permeability channels was very useful in the investigated hydrogeological setting. As one of the main groundwater discharge outlets of the Pantano Formation, this study has highlighted the key role of enlarged tectonic and layer-parallel fractures for locally enhanced hydraulic connectivity (Gellasch et al, 2013) within the aquifer. Nanoparticles arrived very rapidly at three distinct points following different directions from the injection point; the convergence of groundwater flow toward the main outlet of the system appears to be accomplished thanks to the enlargement of existing fractures in the calcite-rich aquifer unit, most likely occurring through karst dissolution processes. Therefore, the aquifer, that was previously considered to be dominated by fracture flow, based on previous knowledge of sandstones in area, is most likely behaving as a karst-like system with all the yield concentrated in relatively few conduits. The effective groundwater velocity estimated through the breakthrough curves is around one order of magnitude higher compared to previous experimental values determined in fractured turbiditic sandstones. This explains the hydrogeological relevance of PAT as a regional strategic groundwater reservoir.

This research demonstrates that a tracer test using DNA labelled nanoparticles can be valuable for defining groundwater effective transport velocity in the discharge area of main aquifers. This could support the delimitation of spring-head protection zones through chronological or modelling tools. The test site ranges from 5 to 70 m in both lateral extent and depth. The applicability of nanoparticle tracers for larger scales is still questionable due to their tendency to settleand their limited mobility across low-velocity zones. Further research is needed to create more realistic expectations regarding the use of nanoparticles for the characterization of larger systems.

**Acknowledgments**

The authors express their gratitude to Dr. Stefano Segadelli (geologic service of Emilia-Romagna region) for his precious support in the field. They also extend their acknowledgements to GruppoHera s.p.a. water company whose technical and funding support made this investigation possible.

**Statement about conflict of interest**

On behalf of all authors, the corresponding author states that there is no conflict of interest.

**References**

Albarran N, Missana T, Alonso U, García-Gutiérrez M, López T (2013) Analysis of latex, gold and smectite colloid transport and retention in artificial fractures in crystalline rock, Colloids and Surfaces A: Physicochemical and Engineering Aspects, 435: 115–126.

Aquilanti L, Clementi F, Nanni T, Palpacelli S, Tazioli A,Vivalda PM (2016) DNA and fluorescein tracer tests to study the recharge, groundwater flowpath and hydraulic contact of aquifers in the Umbria-Marche limestone ridge (central Apennines, Italy), Environmental Earth Sciences, 75:626

Bailly-Comte V, Durepaire X, Batiot-Guilhe C, Schnegg PA (2018) In situ monitoring of tracer tests: How to distinguish tracer recovery from natural background, Hydrogeology Journal, 26: 2057–2069.

Barker AP, Newton RJ, Bottrell SH, Tellam JH (1998) Processes affecting groundwater chemistry in a zone of saline intrusion into an urban sandstone aquifer, Applied Geochemistry 13(6):735–749.

Bettelli G, Panini F, Pizziolo M (2002) Explanatory notes of Geological Map of Italy, 1:50.000 scale. Sheet 236 Pavullo nel Frignano (in italian). Geological Service of Italy, Emilia-Romagna Region, S.EL.CA. printer, Florence (Italy). https://www.isprambiente.gov.it/Media/carg/note_illustrative/236_Pavullo_nel_Frignano.pdf

Carminati E & Doglioni C (2012) Alps vs. Apennines: The paradigm of a tectonically asymmetric Earth, Earth-Science Reviews, 112(1–2):67–96.

Castellarin A (2001) Alps-Apennines and Po Plain-Frontal Apennines relationships. In: Vai GB & Martini IP (eds) Anatomy of an Orogen. The Apennines and adjacent Mediterranean Basins, Springer, London, p 177-196.

Chuang P, Chia Y, Liou Y, Teng M, Liu C, Lee T (2016) Characterization of preferential flow paths between boreholes in fractured rock using a nanoscale zero-valent iron tracer test, Hydrogeology Journal, 24:1651-1662.

Chrysikopoulos CV & Katzourakis VE (2015) Colloid particle size-dependent dispersivity, Water Resources Research, 51:4668–4683.

Colleuille H & Kitterod NO (1998) Forurensning av drikkevannsbronn pâ Sundreoya i Âl kommune. Résultat av sporstoff-forsok (transl.: Pollution of Drinking Water Well on Sundreoya in Âl Municipality. Results of Trace Element Experiment). Norwegian Water Resources and Energy Directorate Report 18 (inedit Report, in Norwegian).

Dahlke HE, Williamson AG, Georgakakos C, Leung S, Sharma AN, Lyon SW, Walter MT (2015) Using concurrent DNA tracer injections to infer glacial flow pathways, Hydrological Processes, 29:5257−5274.

Divine CE & McDonnell JJ (2005) The future of applied tracers in hydrogeology, Hydrogeology Journal, 13(1): 255–258.

Fahrmeier N, Goeppert N, Goldscheider N (2021) Comparative application and optimization of different single-borehole dilution test techniques, Hydrogeology Journal, 29:199–211.

Fetter CW (2018) Applied Hydrogeology, Waveland Press Inc., Long Grove

Filippini M, Segadelli S, Dinelli E, Failoni M, Stumpp C, Vignaroli G, Casati T, Tiboni B, Gargini A (2024) Hydrogeological assessment of a major spring discharging from a calcarenitic aquifer with implications on resilience to climate change,Science of the Total Environment, https://doi.org/10.1016/j.scitotenv.2023.169770.

Foppen JW, Orup C, Adell R, Poulalion V, Uhlenbrook S (2011) Using multiple artificial DNA tracers in hydrology, Hydrological Processes, 25:3101-3106.

Foppen J W, Seopa J, Bakobie N, Bogaard T (2013) Development of a methodology for the application of synthetic DNA in stream tracer injection experiments, Water Resources Research, 49:5369−5380.

Gargini A, Vincenzi V, Piccinini L, Zuppi GM, Canuti P (2008) Groundwater flow systems in turbidites of Northern Apennines (Italy): natural discharge and high speed railway tunnels drainage, Hydrogeology Journal, 16(8):1577-1599.

Gellasch CA, Bradbury KR, Hart DJ, Bahr JM (2013) Characterization of fracture connectivity in a siliciclastic bedrock aquifer near a public supply well (Wisconsin, USA), Hydrogeology Journal, 21(2):383–399.

Georgakakos CB, Richards PL, Walter MT (2019) Tracing septic pollution sources using synthetic DNA tracers: proof of concept, Air Soil Water Research, 12, doi:1.1178622119863794.

Grindrod P, Edwards MS, Higgo JJW, Williams GM (1996) Analysis of colloid and tracer breakthrough curves, Journal of Contaminant Hydrology, 21(1–4):243–253.

Harvey RW & Garabedian SP (1991) Use of colloid filtration theory in modeling movement of bacteria through a contaminated sandy aquifer, Environmental Science and Technology, 25(1):178–185.

James SC & Chrysikopoulos CV (2011) Monodisperse and polydisperse colloid transport in water-saturated fractures with various orientations: Gravity effects, Advances in Water Resources, 34:1249–1255.

Käss W (1998) Tracing technique in geohydrology. Balkema, Rotterdam.

Keegan-Treloar R, Irvine DJ, Solòrzano-Rivas SC, Werner AD, Banks EW, Currell MJ (2022) Fault-controlled springs: A review, Earth-Science Reviews, 230, doi.org/10.1016/j.earscirev.2022.104058

Kitteröd NO, Colleuille H, Pedersen TS, Langsholt E, Dimakis P (1998) Vanntransport i oppsprukket fjell. Numeriske simuleringer av vannlekkasjer i Romeriksporten (transl.: Water Transport in Fractured Rocks: Numerical Simulations of Water Leaks in the Romeriksporten Tunnel), Norwegian Water Resources and Energy Directorate Report 11 (inedit report, in Norwegian).

Kittilä A, Jalali MR, Evans KF, Willmann M, Saar MO, Kong XZ (2019) Field comparison of DNA-labeled nanoparticle and solute tracer transport in a fractured crystalline rock, Water Resources Research, 55:6577–6595.

Kong XZ, Deuber CA, Kittilä A, Somogyvári M, Mikutis G, Bayer P, Stark WJ, Saar MO (2018) Tomographic reservoir imaging with dna-labeled silica nanotracers: The first field validation, Environmental Science & Technology, 52(23):13681–13689.

Leibundgut C, Maloszewski P, Külls C (2009) Tracers in Hydrology. John Wiley & Sons.

Liao R, Yang P, Wu W, Luo D, Yang DA (2018) DNA tracer system for hydrological environment investigations, Environmental Sciences & Technology, 52, doi:10.1021/acs.est.7b02928

McKay L, Sanford W, Strong J (2000) Field-scale migration of colloidal tracers in a fractured shale saprolite, Ground Water, 38(1):139–147.

McNew CP, Wang C, Walter MT, Dahlke HE (2018) Fabrication, detection, and analysis of DNA-labeled PLGA particles for environmental transport studies, Journal of Colloid and Interface Science, 526:207–219.

Medici G, West LJ, Mountney NP (2016) Characterizing flow pathways in a sandstone aquifer: Tectonic vs sedimentary heterogeneities, Journal of Contaminant Hydrology, 194:36-58.

Meinzer OE (1923) The Occurrence of GroundWater in United States with a discussion of principles, USGS Water-Supply Paper 489, Washington.DC, USA.

Mikutis G, Deuber CA, Schmid L, Kittilä A, Lobsiger N, Puddu M, Asgeirsson DO, Grass RN, Saar MO, Stark WJ (2018) Silica-Encapsulated DNA-Based Tracers for Aquifer Characterization, Environmental Science and Technology, 52:12142-12152.

524 Mora CA, Paunescu D, Grass RN, Stark WJ (2015) Silica particles with encapsulated DNA as trophic tracers,
525 Molecolar Ecology Resources, 15:231-241.

526 Ori GG & Friend PF (1984) Sedimentary basins formed and carried piggyback on active thrust sheets, Geology,
527 12(8):475–478.

528 Pang L, Robson B, Farkas K, McGill E, Varsani A, Gillot L, Li J, Abraham P (2017) Tracking effluent discharges
529 in undisturbed stony soil and alluvial gravel aquifer using synthetic DNA tracers, Science of the Total
530 Environment, 592:144.152.

531 Pang L, Abeysekera G, Hanning K, Premaratne A, Robson B, Abraham P, Sutton R, Hanson C, Hadfield J,
532 Heiligenthal L, Stone D, McBeth K, Billington C (2020) Water tracking in surface water, groundwater and soils
533 using free and alginate-chitosan encapsulated synthetic DNA tracers, Water Research, 184:116192.

534 Panini F, Bettelli G, Pizziolo M (2002) Explanatory notes of Geological Map of Italy, 1:50.000 scale. Sheet 237
535 Sasso Marconi (in italian). Geological Service of Italy, Emilia-Romagna Region, S.EL.CA. printer, Florence.
536 https://www.isprambiente.gov.it/Media/carg/note_illustrative/237_Sasso_Marconi.pdf

537 Paunescu D, Puddu M, Soellner JOB, Stoessel PR, Grass RN (2013) Reversible DNA encapsulation in silica to
538 produce ROS-resistant and heat-resistant synthetic DNA 'fossils', Nature Protocols, 12:2440–2448.

539 Petitta M, Banzato F, Lorenzi V, Matani E, Sbarbati C (2022) Determining recharge distribution in fractured
540 carbonate aquifers in central Italy using environmental isotopes: Snowpack cover as an indicator for future
541 availability of groundwater resources, Hydrogeology Journal, 30:1619–1636.

542 Piccinini L, Fabbri P, Pola M (2016) Point dilution tests to calculate grownd water velocity: an example in a porous
543 aquifer in northeast Italy, Hydrological Sciences Journal, 61(8):1512-1523.

544 Ptak T, Piepenbrink M, Martac E (2004) Tracer tests for the investigation of heterogeneous porous media and
545 stochastic modelling of flow and transport-a review of some recent developments, Journal of Hydrology, 294:
546 122–163.

547 Sabir IH, Haldorsen S, Torgersen J, Aleström P, Sabir IH, Haldorsen S (1999) DNA tracers with information
548 capacity and high detection sensitivity tested in groundwater studies, Hydrogeology Journal, 7:264–272.

549 Sabir IH, Haldorsen S, Alestrom P (2001) Use of Synthetic DNA as New Tracers for Tracing Groundwater Flow
550 and Multiple Contaminants, Journal of Applied Sciences, 1:233-238.

551 Segadelli S, Filippini M, Monti A, Celico F, Gargini A (2021) Estimation of recharge in mountain hard rock
552 aquifers based on discrete spring discharge monitoring during base-flow recession, Hydrogeology Journal, 29(3),
553 949-961.

554 Sharma AN, Luo D, Walter MT (2012) Hydrological tracers using nanobiotechnology: proof of concept.
555 Environmental Science and Technology, 46:8928-8936.

556 Sirivithayapakorn S & Keller A (2003) Transport of colloids in saturated porous media: A pore-scale observation
557 of the size exclusion effect and colloid acceleration, Water Resources Research, 39(4),
558 https://doi.org/10.1029/2002WR001583.

559 Wang T & He N (2010) Preparation, characterization and applications of low molecular weight alginate–
560 oligochitosan nanocapsules, Nanoscale 2(2):230–239.

561 Zhuang J, Tyner JS, Perfect E (2009) Colloid transport and remobilization in porous media during infiltration and
562 drainage, Journal of Hydrology, 377(1):112−119.

563 Zvikelsky O, Weisbrod N, Dody A (2008) A comparison of clay colloid and artificial microsphere transport in
564 natural discrete fractures, Journal of Colloid Interface Science, 323(2):286−292.

565

## DECLARATIONS

* Ethics approval and consent to participate

Not applicable

* Consent for publication

As corresponding author and on behalf of other co-authors I consent for the publication of the presented paper on Hydrogeology Journal

* Availability of data and material

The analytical data relative to tracer recovery are all presented in the paper

* Competing interests

Not applicable

* Funding

The research was financed partly by GruppoHera s.p.a. water company and partly by free use funding (resp. prof. Alessandro Gargini) of the Department of Biological, Geological and Environmental Sciences of the University of Bologna.

* Author Contribution

**Ernesto Pugliese**: conceptualization and methodology, technical designing and planning of tracer test in the field, investigation, visualization, writing – review & editing.; **Cristina Giuliani**: Conceptualization and Methodology of DNA analysis, Data interpretation, writing – review & editing.; **Giorgia Bolognesi**: Methodology of DNA analysis, Data Interpretation; **Maria Filippini**: conceptualization and formal analysis, writing – review & editing; **Matteo Barbero**: investigation, methodology, technical support in the field for NaCl tracer test; **Marjan Edahie**: investigation, technical support in the field and in the lab for DNA tracer test; **Alessandro Gargini**: general scientific coordination, conceptualization, writing-original draft.

## FIGURE CAPTIONS

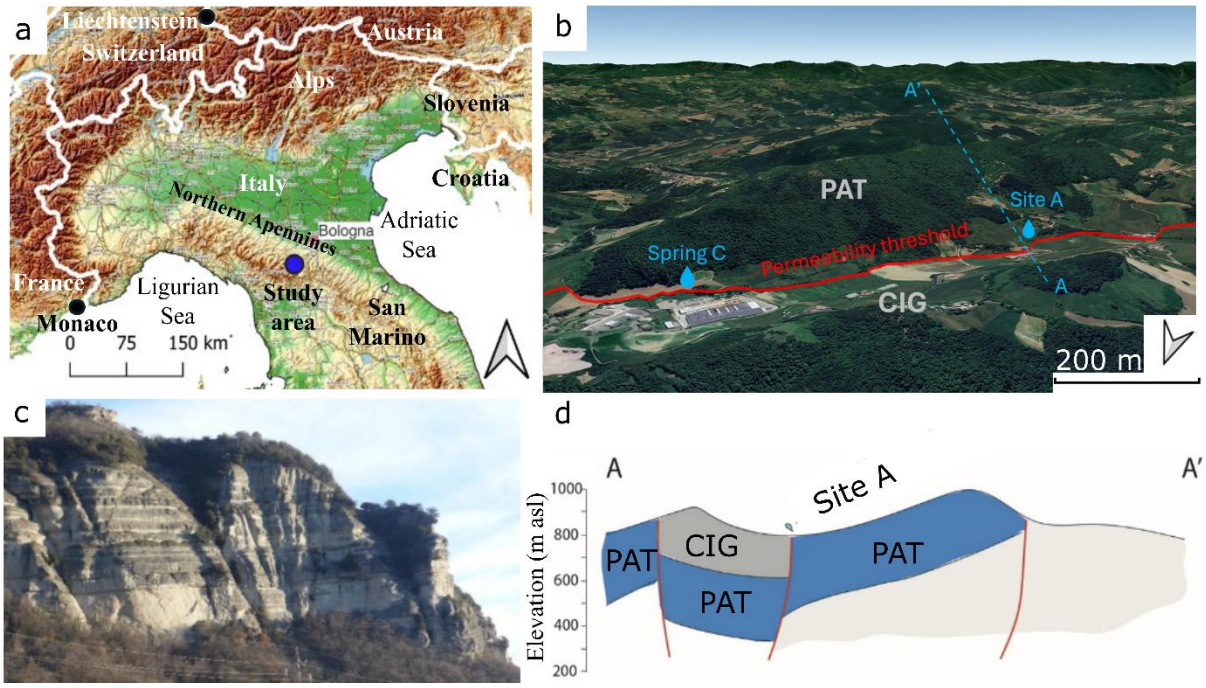


**Fig.1** a) Location of the study site (*blue dot*) in the Northern Apennines, Italy; b) Oblique view (from northwest) of the Arpolli Slab relief, developed on the Pantano Formation (PAT), surrounded by marly-clayey units of the Cigarello Formation (CIGF). In the background, the main divide of the Apenninic chain is visible; c) Outcrop of PAT calcarenitic aquifer unit in a cliff nearby Site A (Photograph of Dr.Phd Stefano Segadelli); d) Hydrogeological profile along the trace *A-A'* with the aquifer unit *in blue*.

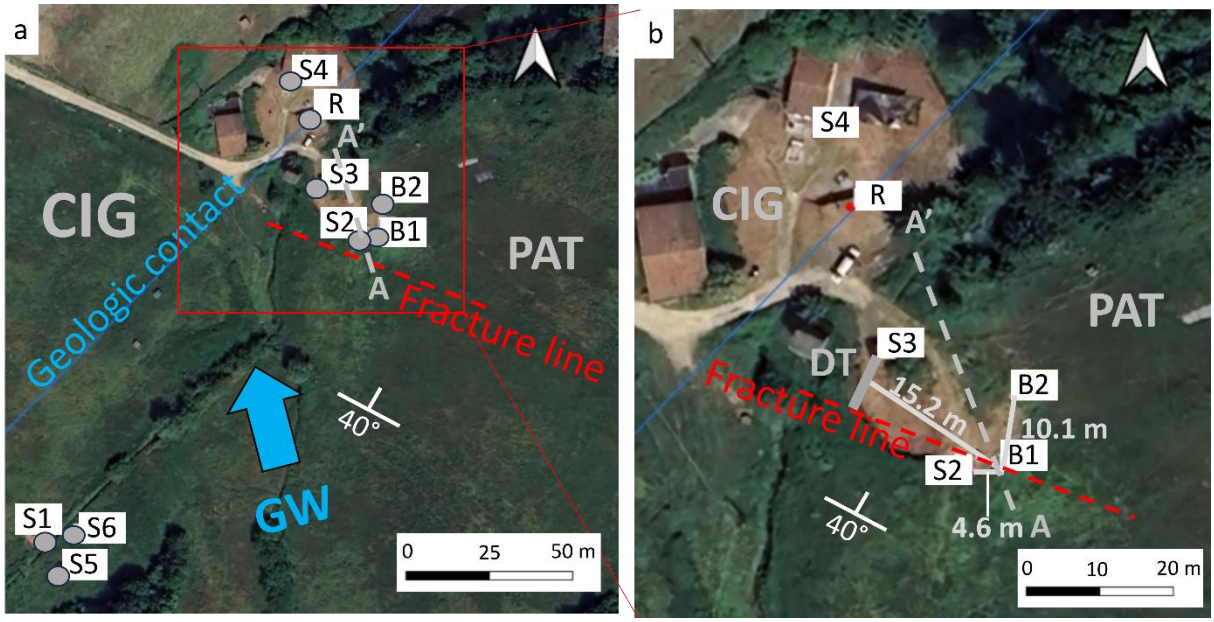


**Fig.2** a) Detailed map of Site A on a Google-Earth base. Spring boxes are coded with *S*, boreholes are coded with *B*. *R* indicates the reservoir building, *GW* stands for mean groundwater flow direction, *PAT* and *CIG* stand for outcropping areas of the Pantano and Cigarello formations, respectively. Disposition of strata below the ground surface is indicated (*in white*) as determined in borehole B1 and B2 by lithology logs; b) Enlargement of the map *a* with the location of injection and sampling points for the tracer test along with the distances between them. *DT*

605 marks the trace of the drainage tunnel associated with spring *S3*. Symbols are consistent with those marked in map
606 *a*. The line A'-A corresponds to the cross-section illustrated in Fig.3.

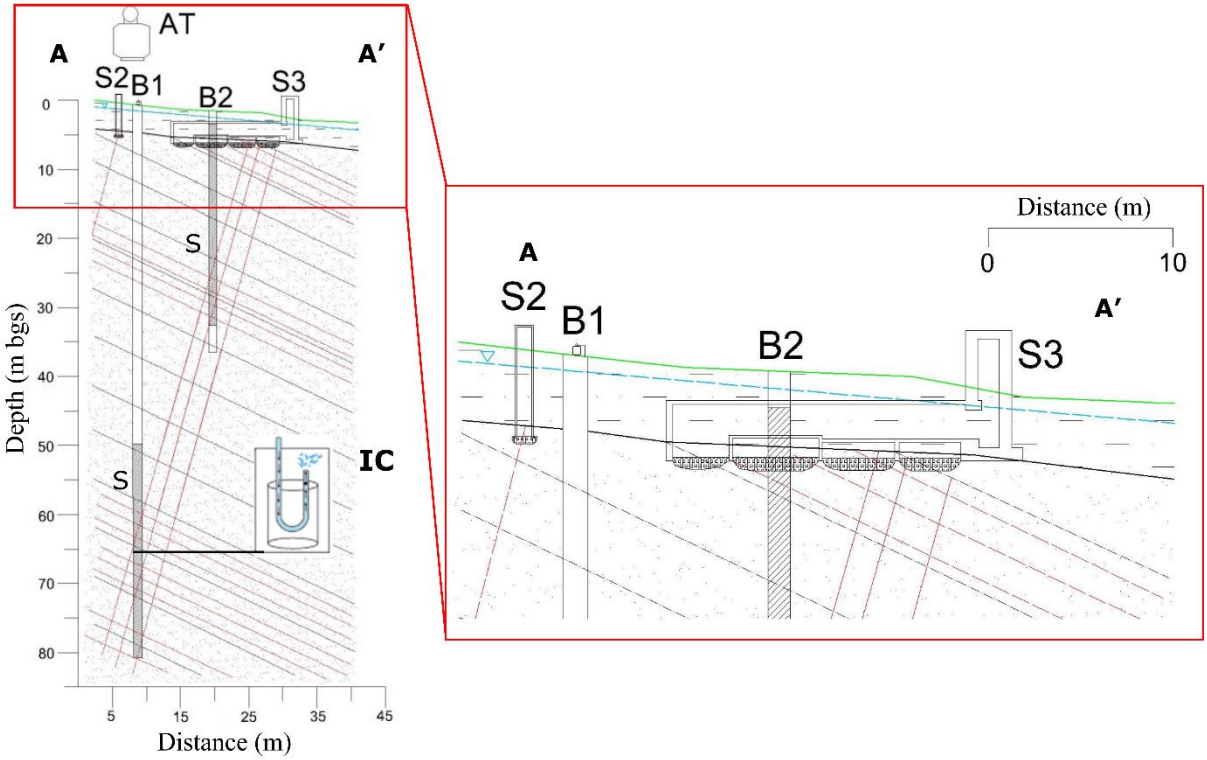


607

608 **Fig.3** Cross-sections of Site A along line *A-A'* (of Fig.2). The right section is an enlargement of the left section.
609 Disposition of strata within the PAT Formation is indicated *in grey lines*; tectonic and layer-parallel fractures are
610 indicated by *red lines*. Vertical shaft and draining tunnel of spring boxes *S2* and *S3* are drawn to scale according
611 to their real design. Explanation of symbols: *AT*: Air Tank; *IC*: Injection Chamber; *S*: Borehole Screen.

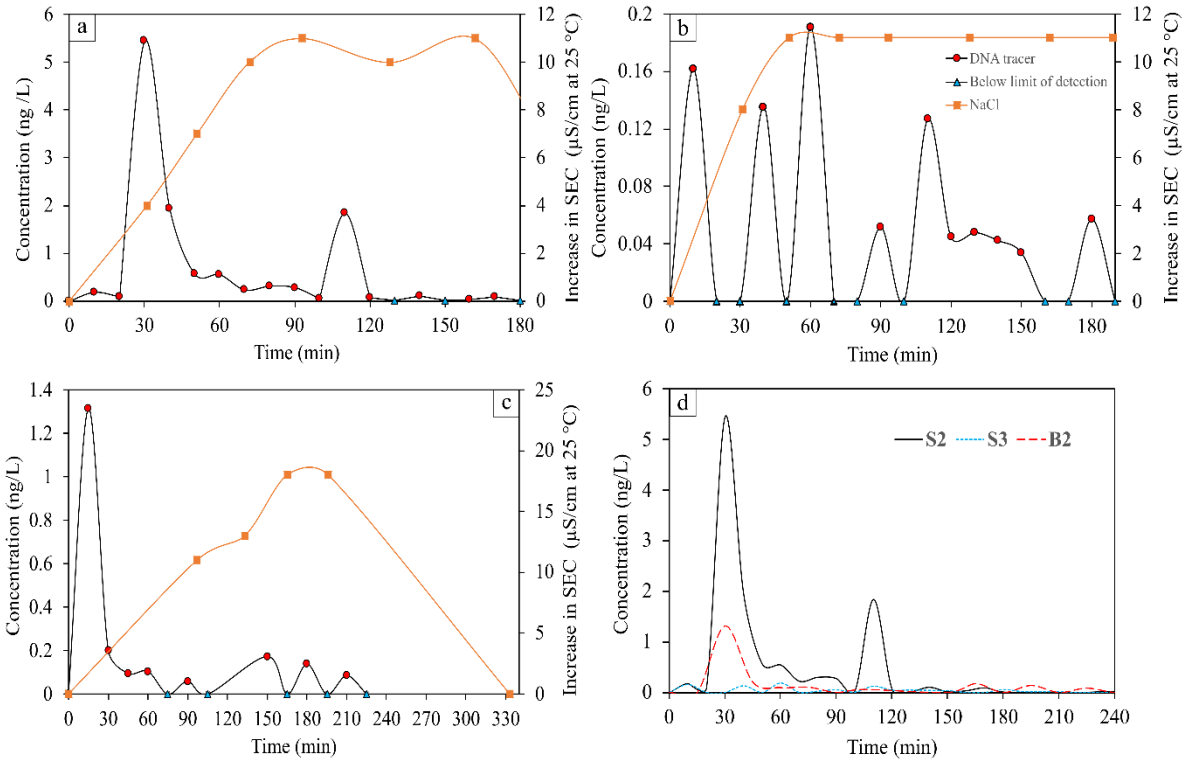


612

613 **Fig.4** Breakthrough curves obtained in S2, S3, B2 for nanoparticles (left-hand axis, *gray curve*) and for NaCl,
614 expressed as increase in specific electrical conductance (SEC) at 25°C (right-hand axis, *orange curve*). The lower
615 right graph shows a comparison between the three curves for DNA. Samples resulting with a concentration of
616 nanoparticles considered as null or lower than the detection limit ($2.64\times10^{-2}$ ng/L) are considered as non-detects
617 and labelled *in blue* whereas detected outcomes are labelled *in red*.

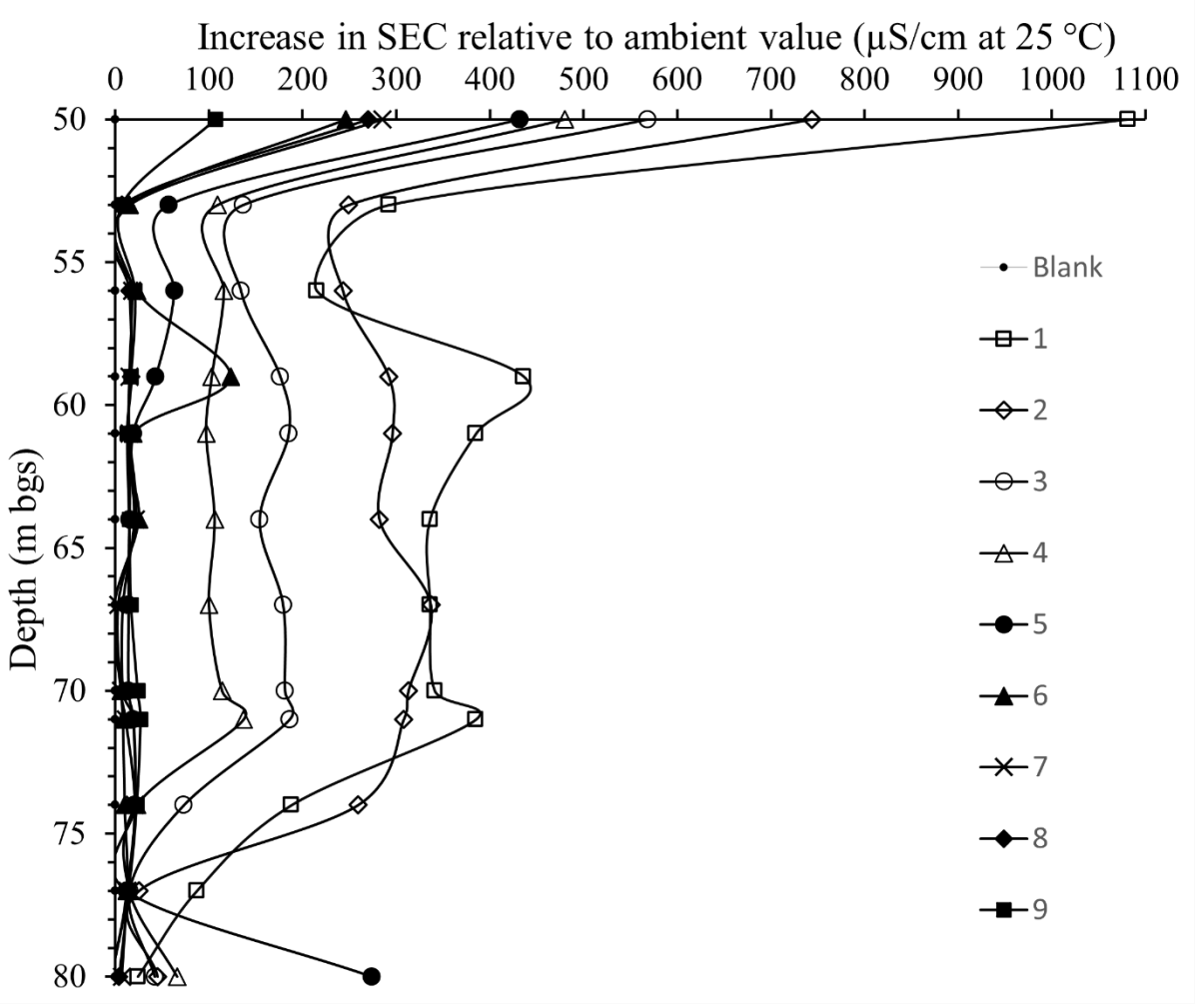


**Fig.5** Borehole dilution test (BDT) in borehole B1: vertical specific electrical conductivity (SEC) log obtained by the profiler along the screen of borehole. The depth on the y axis is in m below ground surface. The numbers *from 1 to 9* indicate the temporal order of the profiles from *1* (immediately after the injection) to *9* (6 hours after injection). Zones with fracture enlargement are shown *in red*.

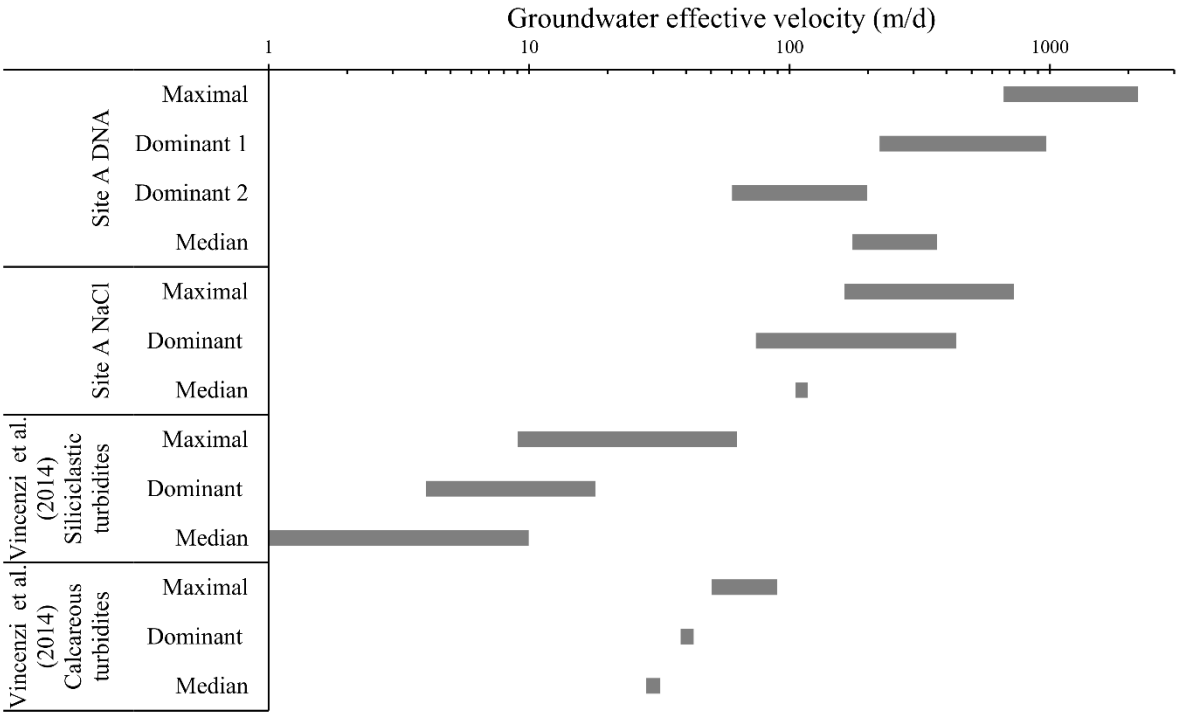


**Fig.6** Ranges of values for components of groundwater effective velocity (m/d) (see *Groundwater effective flow velocities* in the *main text* for further explanation) as derived from the tracer test presented in this study and from Vincenzi et al. (2014) injecting fluorescent dyes in arenitic turbidite aquifers.